Geophys. J. R. astr. Soc. (1977) 51.

The coercive force spectrum of magnetite at high temperatures, evidence for thermal activation below the blocking tempemture

David J. Duhlop *Geophysics Laboratory, Department of Physics, University of Toronto, Toronto, Canada*

Mohammad-Mansour Bina, *Département de Physique, Faculté des Sciences, Université de Téhéran, Téhéran, Iran*

Kcceived 1977 February 15; in original tritm 1976 October 12

Summary. Thermal activation of magnetization is the mechanism proposed by Neel to explain TRM (thermoiomancnt magnetization) and VRM (viscous rcmancnt magnetization). Ned's thcoiy is difficult to test because in a small constant field, magnetization changes occur only at or near particle blocking temperatures. By increasing the field, the blocking temperature can be lowered to any desired temperature, including room temperature. Isothermal hysteresis or demagnetization data, paiticulaily coercive forces, therefore provide information about thermal fluctuations at temperatures well below the usual blocking temperatures of low-field TRM or VRM.

We apply *thermal fluctuation analysis* (Dunlop) to high-temperature measurements of average coercive force and of the coercive force spectrum (from alternating-field demagnetization). The samples incorporate representative fractions (average grain sizes from 0.04 to 0.22 μm) of the lower pseudo-single-domain (PSD) range of magnetite and one fraction (1–5 μm size spread) from the upper PSD range. The ordinary coercive force H_C has the same temperature dependence as the softest 20–30 per cent of the coercive force spectrum, whereas the remanent coercive force H_R has the same temperature dependence as the median demagnetizing field. H_R is, therefore, a more meaningful average over the coercive force spectrum than H_C. The predicted dependence of Néel's 'fluctuation field' H_q on temperature, on grain size and on microscopic coercive force H_K are followed quite closely by the smaller PSD grains, but not by the 1–5 μm grains. By extrapolation, the critical size for (room-temperature) superparamagnetic behaviour in magnetite is found to be (250^{+25}_{-10}) Å, in good agreement with previous experimental and theoretical estimates.

On the basis of fluctuation analysis, domain walls with a minimum width ~0.1 μm carry the permanent magnetic moment of small multidomain magnetite grains. This wall moment, thermally activated as a unit, rotates in

single-domain-like fashion. Wall displacement plays a secondary role in two-domain particles, at least in those < 0.22 μm in size: fluctuation fields at the TRM blocking temperature, as inferred from the Néel wall displacement model of TRM, are inconsistent with observed (and predicted) magnitudes and size variation of H_q. However, in 1–5 μm grains, although PSD moments are generally accepted as the explanation of their enhanced low-field TRM intensity, hysteresis and alternating-field demagnetization results do not give unequivocal evidence of the existence of PSD moments. High-field isothermal magnetic processes in these larger 'PSD' grains are equally well accounted for by wall displacements alone.

1 Introduction

Superparamagnetism, magnetic viscosity, and TRM (thermoremanent magnetization) are classic manifestations of thermal fluctuations in ferromagnetic fine particles. All three are threshold phenomena, in that magnetization changes are thermally activated to a measurable extent only below a critical volume (the superparamagnetic volume, v_s) or above a critical temperature (the blocking temperature, T_B).

This paper shows that thermal activation effects are easily measurable in 'stably' magnetized particles ($v > v_s$, $T < T_B$) when a magnetic field, alternating or steady, comparable to the microscopic coercive force, H_K, is applied. The coercive force, H_C, determined from hysteresis or AF (alternating-field) demagnetization measurements is in effect the 'threshold field' for thermal activation of stable particles. The fluctuation field (Néel 1955), $H_q = H_K - H_C$, is substantial. In 760 Å magnetite particles ($v \approx 25 v_s$) at room temperature, for example, H_C turns out to be 15 per cent lower than the intrinsic or zero-fluctuation coercivity H_K.

High-temperature hysteresis and AF demagnetization measurements are still more strongly influenced by thermal fluctuations. We report data of this type and use the Néel (1949) thermal activation theory to estimate the volume, v_{act}, involved in a single activation event for magnetite particles in two size ranges, 370–2200 Å (0.037–0.22 μm) and 1–5 μm. These particles have multidomain structure, but 'pseudo-single-domain' (PSD) moments (Stacey 1963; Parry 1965) must be invoked to explain the high intensity of low-field TRM (Dunlop, Stacey & Gillingham 1974; Stacey & Banerjee 1974). Comparing v_{act} with grain size observations is a possible means of distinguishing between domain wall activation and activation of PSD moments.

2 Thermal fluctuation theory

2.1 MICROSCOPIC COERCIVE FORCE

In the absence of thermal fluctuations (i.e. at 0 K), a single-domain (SD) particle exhibits step-function response to an applied magnetic field H. The threshold field for domain rotation is H_K, the microscopic coercive force. H_K has two principal sources.

(1) Shape anisotropy of elongated particles: $H_K = \alpha \Delta N J_S$ ($\frac{1}{2} < \alpha < 1$, depending on particle orientation). Here ΔN is the difference between the demagnetizing factors along the shortest and longest particle dimensions and J_S is spontaneous magnetization.

(2) Magnetocrystalline anisotropy: $H_K = \beta |K_1| / J_S$, where K_1 is the first-order anisotropy constant. $\frac{1}{6} < \beta < \frac{4}{9}$ depending on whether domains rotate from the ⟨111⟩ (easy) axis

through ⟨110⟩ (intermediate) or ⟨100⟩ (hard) axes (Stacey & Banerjee 1974, p. 47). Substituting $K_1 = 1.36 \times 10^5$ erg cm^{-3}, $J_S = 485$ emu cm^{-3} for Fe_3O_4, H_K lies between 50 and 370 Oe. The J_S vector will follow the easiest path possible within the constraints of geometry and the direction of H. $H_K \sim 100$ Oe is an intermediate but probably not unreasonable figure.

The effects of shape and crystalline anisotropy are superimposed in any SD particle. However, because ΔN increases rapidly with elongation, shape anisotropy predominates in particles whose longest and shortest dimensions differ by more than about 10 per cent (*cf.* Nagata 1961, p. 70).

At 0 K, multidomain (MD) particles also exhibit stepwise changes in magnetization. Three processes are involved: domain wall motion (low fields), domain rotation (high fields), and nucleation of reverse domains (following saturation). Only the first will concern us. Stacey & Wise (1967) attribute low-field coercivity in MD magnitude to impedance of domain wall motion by dislocations. For a particular Barkhausen jump, they find $H_K = \gamma\lambda\mu/J_S$, where λ is the magnetostriction constant and μ is the shear modulus. γ is a constant of value such that H_K ranges from about 5 Oe (single dislocation) to about 50 Oe (dislocation pile-up). Other approaches are taken by Vicena (1955) and Shive (1969).

Above 0 K, the microscopic coercive force decreases because J_S, K_1, λ and μ are functions of temperature. $J_S(T)$ is well known for magnetite (Pauthenet & Bochirol 1951). K_1 varies approximately as $J_S^{8.5}$ (Fletcher & Banerjee 1969) between 20 and 580°C, the range over which the experiments in this paper were carried out. $\lambda_{111}(T)$ and $\lambda_{100}(T)$ have been measured for magnetite by Klapel & Shive (1974). They decrease somewhat less strongly with temperature than does K_1. $\mu(T)$ presumably increases with temperature but in an unknown way. To summarize

$$H_K(T) \propto \begin{cases} J_S(T) \text{ SD, shape anisotropy} \\ J_S^{n.5}(T) \text{ SD, crystalline anisotropy} \\ J_S^{n}(T)\text{? MD, dislocation pinning} \end{cases} \qquad (1)$$

The temperature dependence quoted for shape anisotropy holds whether domain rotation is coherent or incoherent – e.g. curling mode, Frei, Shtrikman & Treves (1957).

2.2 THERMAL FLUCTUATIONS

The threshold field for magnetization changes decreases with temperature for a second reason, namely thermal agitation. For SD particles, Néel (1949) showed that thermally activated changes must have a characteristic relaxation time

$$\tau = \frac{1}{f_0} \exp\left[\frac{\tfrac{1}{2}\upsilon J_S H_K (1 - |H|/H_K)^2}{kT}\right] \qquad (2)$$

where $f_0 \approx 10^9$ s^{-1} (McNab, Fox & Boyle 1968), υ is particle volume and k is Boltzmann's constant. (Equation (2) is approximate. For an exact analysis see Appendix.) $\tau \approx t$, a typical experimental time, if υ is sufficiently small or T sufficiently high. This is the underlying cause of superparamagnetism, magnetic viscosity and TRM. However, even if $\upsilon > \upsilon_s$, the zero-field superparamagnetic (SPM) threshold, and $T < T_B$, the zero-field blocking temperature, it is clear that τ can be made arbitrarily small by allowing H to approach H_K in equation (2).

The observed coercive force of a particle is therefore a 'threshold field' for thermal activation and may be considerably less than H_K. Now $\tau = t$ when $H = H_C$, whence we have from

equation (2) (Bean & Livingston 1959; Dunlop 1965; Kneller & Wohlfarth 1966)

$$\left.\begin{aligned} H_C &= H_K \left(\frac{2kT\ln(f_0 t)\,H_K}{\upsilon J_S}\right)^{1/2} \\ &= H_K - H_q \end{aligned}\right\} \tag{3}$$

H_q is termed the 'fluctuation field' (Néel 1955). In magnetic viscosity studies, where H is small or zero, H_q has often been called the viscosity field (Néel 1950; see summary in Dunlop 1973a, p. 871). The condition for superparamagnetism is that $H_C = 0$, whence

$$\upsilon_s = 2kT\ln(f_0 t)/J_S H_K,$$

leading to the simpler (but experimentally less useful) expression (Kneller & Luborsky 1963),

$$H_C = H_K(1 - \sqrt{\upsilon_s/\upsilon}). \tag{4}$$

H_K and H_q are different functions of temperature. The temperature dependence of H_C at very low temperatures is due almost entirely to anisotropy, but thermal fluctuations become all-important near T_B. As we shall see, however, H_q is appreciable for $T \ll T_B$, at room temperature for example. Equation (4) indicates that H_q is likewise substantial for particles well above SPM size. For example, if $\upsilon = 10\upsilon_s$, H_q is about 30 per cent of H_K.

Expressions analogous to equation (2) and (3) describe the thermal activation of domain walls in MD particles (Street & Woolley 1949; Néel 1950). Indeed the term 'fluctuation field' was coined by Néel (1955) in connection with MD, not SD, particles. The only changes are that H_K now refers to impedance of domain wall motion and υ is the volume of one Barkhausen jump of the domain wall. (f_0 is slightly different, but it occurs in equation (3) only in a logarithmic term.)

Wohlfarth (1961) points out that equations (2) and (3) describe the thermal activation of still more complex domain structures, provided υ is replaced by υ_{act}, the volume affected by a single activation process. The significance of this observation to rock magnetism is the following. There is a distinctive change in the TRM and initial susceptibility of magnetite particles around a size of 15 μm (Parry 1965). Particles smaller than this size are MD but have only a few domain walls. They are apparently characterized by 'pseudo-single-domain' (PSD) magnetic moments which impart a remanent magnetization intermediate in intensity and coercivity between that of SD and large MD particles. The nature of these moments and the process by which they change their magnetic state are uncertain. Among the suggestions have been Barkhausen discreteness of wall positions (Stacey 1963), domain-wall moments in two-domain grains (Dunlop 1973b; Stacey & Banerjee 1974) and regions of SD size surrounding surface defects in larger grains (Stacey & Banerjee 1974). Depending on the mechanism, $H_K(T)$ may be SD-like, MD-like, or something quite unknown. υ_{act} is quite different for the different mechanisms and provides a possible means of choosing one model over the others.

2.3 THE COERCIVE FORCE SPECTRUM

No real sample exhibits a single coercive force. AF demagnetization, DC magnetization (i.e. IRM) and 'DC demagnetization' (Roquet 1954) curves all indicate a spectrum of coercive forces. The spectrum arises for three reasons.

(1) In both SD and MD particles, H_K depends on the orientation of the applied field relative to the magnetization.

(2) The internal demagnetizing field (MD case) or the interaction field of other particles (SD case) is added vectorially to the applied field.

(3) There is a grain distribution $f(v, H_K)$ (Néel 1949; Dunlop 1965), reflecting the distribution of sizes and shapes of SD particles or the distribution of Barkhausen jumps and barriers to wall motion in MD particles.

The first effect can, in principle, be calculated for randomly oriented particles. The second effect is not calculable and, despite its importance, is generally ignored. On the assumption (a poor one for MD particles) that the distributions of orientations and internal fields are about the same for all (v, H_K), the coercivity spectrum observed experimentally, via AF demagnetization for example, largely reflects the grain distribution $f(v, H_K)$. Near 0 K, it would reflect $f(H_K)$ only, but at normal temperatures, H_c depends (equation (3)) on v as well as H_K.

2.4 TESTS OF THE THEORY

The Néel (1949) theory has been difficult to test because $f(v, H_K)$ is never known in detail. Dunlop & West (1969) examined total and partial TRM and VRM (viscous remanent magnetization) data. Since TRM and VRM are threshold phenomena, the observed spectra of decay times and demagnetizing temperatures and fields are not intrinsic to the phenomena but merely reflect $f(v, H_K)$. In deconvolving the results, Dunlop & West were forced to use a grain distribution inferred from other magnetic measurements. Theirs was, therefore, a necessary, but not a sufficient, test of the theory.

In equations (3) and (4), we have the possibility of a fundamental test of the Néel theory. Equation (3) describes an effect intrinsically observable, for a single (v, H_K), over a broad range of T and not at a single threshold temperature. Dunlop (1976) has described the analysis of high-temperature coercive force data in the light of equation (3), a process he terms 'thermal fluctuation analysis'. Similarly equation (4) covers a broad range of v for a single T. The grain distribution of course still tends to spread the data but the intrinsic trends of equation (3) and (4) should be observable if the following conditions hold (*cf.* Dunlop 1976).

(1) H_K has the same temperature dependence everywhere in the coercivity spectrum (e.g. all particles have the same type of anisotropy).

(2) $\phi(v)$ is reasonably narrow and is the same everywhere in the coercivity spectrum, i.e. $f(v, H_K) = \phi(v)\,\psi(H_K)$.

(3) Experiments are confined to temperatures below the lowest T_B of the sample (equivalently, $v > v_s$ for all particles).

These conditions are experimentally realizable by careful selection of samples and design of experiments. The effect of $\phi(v)$ can then be simulated by replacing v in equations (3) and (4) by a suitable average $\langle v \rangle$ and the effect of $\psi(H_K)$ by examining either some average over the coercive force spectrum (e.g. bulk coercive force) or various fractions of the spectrum separately. Both approaches are described in the present paper.

Kneller & Luborsky (1963) tested equation (4) using bulk coercive force measurements at 4, 77 and 207 K. The fits were convincing for SD iron–cobalt particles, less so for SD iron particles with broader $f(v, H_K)$. Deviations from the simple theory were particularly evident when $v \sim v_s$, in violation of condition (3) above.

Kneller & Wohlfarth (1966) compared the difference ΔH_0 in H_1 values at 77 and at 300 K, determined from AF demagnetization curves at these temperatures, with the predictions of equation (3). Agreement was reasonable provided ΔH (H is peak AF) was ascribed

entirely to ΔH_q. That is, H_K was assumed not to vary appreciably between 77 and 300 K. The result is suspect because we have argued that ΔH_K probably outweighs ΔH_q in the low-temperature thermal variation of H_c. Kneller & Wohlfarth also noted that for different fractions of the coercivity spectrum ΔH_q (i.e. ΔH in their experiments) varied approximately as $H^{1/2}$, as equation (3) predicts.

Gustard & Köster (1967, 1968) compared both DC magnetizing and 'DC demagnetizing' curves of IRM at 20 and at 70 or 80°C for seven dispersions of SD γFe_2O_3 and CrO_2. Like Kneller & Wohlfarth, they did not in general attempt to separate $H_q(T)$ from $H_K(T)$. For one coercivity fraction of one sample, they attempted a separation over the range 77–420 K (shape anisotropy was assumed) and found $H_q = 84$ Oe at room temperature, as compared with the 35 Oe predicted. Their average grain size, however, was uncertain by a factor 3. This uncertainty could account for most of the disagreement.

Both Gustard & Köster (1967, 1968) and Kneller & Wohlfarth (1966) ultimately chose a pair of temperatures at which they compared coercive force data. Dunlop (1976) instead tested the temperature dependence of H_q (assuming shape anisotropy in making the separation from H_K) at six temperatures between 20 and 560°C. His samples SD2 and SD3 contained elongated SD particles of magnetite, natural in one case, synthetic in the other. The predicted temperature dependence was followed and $\langle v \rangle$ values from the curve-fitting were reasonable, although the grain distribution was not known very accurately.

It is apparent that all the previous experiments, while they substantiate the theory in a general way, leave something to be desired. In some cases, the effects of $H_q(T)$ and $H_K(T)$ were not separated. In others, it is clear that a substantial fraction of particles unblock between the lowest and highest temperatures used. In all cases, uncertainty in the mean grain size compromises the results. For these reasons, particular care was taken in the present experiments to use only samples with well characterized and narrow grain distributions, so as to ensure an accurately defined $\langle v \rangle$, and a narrow spectrum of T_B's confined to temperatures well above room temperature.

3 Experimental procedure

3.1 PROPERTIES OF THE SAMPLES

Experiments were carried out on four vacuum-sealed 1 per cent dispersions of slightly (3–15 per cent) non-stoichiometric magnetite crystals, roughly cubic in shape. The preparation and properties of these magnetites are described in detail by Dunlop (1973b,c). Properties germane to the present experiments are given in Table 1 in the next section. The grain size distribution is known with fair precision from electron microscopy. Mean particle sizes, by this method and from surface area measurements by BET nitrogen adsorption (Adamson 1967, pp. 506–8), range from 2200 Å (0.22 μm) for sample 1 to 370 Å (0.037 μm) for sample 4. The distributions are relatively narrow. Standard deviations σ_d about the mean size are 25–40 per cent. By comparison, in the only previous study where size distributions were determined, Gustard & Köster (1968) found >100 per cent standard deviations for their commercial-grade γFe_2O_3 powders.

The mean sizes quoted for samples 1–4 are actually upper limits. The particles consisted initially of a core (85–97 per cent of the particle volume) of Fe_3O_4 and a surface layer near γFe_2O_3 in composition. After 750°C vacuum annealing, designed to stabilize magnetic properties in subsequent heatings, saturation magnetization decreased in proportion to the initial non-stochiometry, as γFe_2O_3 inverted to practically non-magnetic αFe_2O_3.

Heat treatment had little effect on the particle sizes or conditions of internal stress in samples 1–3. Their structure-sensitive properties scarcely changed with heating. On the

other hand, the bulk coercive force of sample 4 increased about 30 per cent after heating. Unlike the other samples, sample 4 contained a sizeable fraction of SPM particles. The finest of these were probably initially wholly oxidized to γFe_2O_3 and inverted upon heating. The larger SPM particles may have grown to stable SD size. Even after heating, blocking temperatures in sample 4 are widely distributed, from 550°C down to 20°C. The T_B spectra of samples 1–3 are narrow (Table 1 and Fig. 1). Despite its drawbacks, however, sample 4 was retained in the study because it is the only sample that contains primarily SD material. Virtually all particles in samples 1–3 are larger than 500 Å, the critical SD size for magnetite (Dunlop 1973c). Their values of J_{rs}/J_S (J_{rs} is saturation IRM) range from 0.113 to 0.242, only 20 to 50 per cent that of randomly oriented SD particles.

In a later section, we analyse the results of experiments carried out by Bina (1971) on a vacuum-sealed 3 per cent dispersion of very pure magnetite particles. Fe_3O_4 was produced by decomposition of FeO at moderate temperatures. The FeO matrix was then dissolved and the Fe_3O_4 particles recovered electrolytically (Bina, Manenc & Voeltzel 1966). This technique yields strain-free particles with a narrower size distribution than grinding and centrifugal separation (Parry 1965; Gillingham & Stacey 1971). Bina's sample is not as well characterized as samples 1–4, but the particles are in the 1–5 μm size range, below the PSD threshold of 15–20 μm (Parry 1965; Bailey 1975).

3.2 EXPERIMENTS AND INSTRUMENTATION

The key experiments in this paper are high-temperature hysteresis and AF demagnetization. Since all fields were applied and all measurements were made at elevated temperatures, a specialized instrument incorporating a ballistic magnetometer, whose sensitivity was enhanced by a feedback amplifier, a high-field solenoid (AC to 3 kOe peak, DC to 2.3 kOe) and a furnace was used (West & Dunlop 1971). Bina used very similar equipment for his experiments (Bina 1966).

4 Activation volumes from blocking temperature data

Dunlop (1973b) reported blocking-temperature data and $\langle v_{act} \rangle$ for samples 1–4. These results will be reviewed briefly because they set the stage for what follows. By substituting $\tau = t$ if $T = T_B$, equation (2) becomes a formula for v_{act} in terms of T_B, as observed in the thermal demagnetization of TRM. Fig. 1(a) reproduces the appropriate experimental results. The blocking temperatures of samples 1–3 are confined to a narrow range below the Curie point and above 545°C.

To calculate v_{act}, we need to know how H_K varies with temperature (*cf.* equations (1)) and its value H_{K0} at one reference temperature. Dunlop assumed $H_K(T) \propto J_S(T)$. This turns out, as we will see later in this section, to be a reasonable description, despite the fact that the particles are neither elongated nor, for the most part, SD. Substituting for H_{K0} at 20°C $\tilde{H}_{1/2}$, the median demagnetizing field of 1-Oe TRM (we will obtain better estimates of H_{K0} later), one obtains the mean activation sizes given in Table 1.

The figures for $\langle d_{act} \rangle$ are unweighted arithmetic averages of the activation sizes corresponding to minimum and maximum values of T_B. Even though the range of T_B is only 10–20°C in samples 1–3, the range of d_{act} is 200–300 Å and the method of averaging is important. For sample 4, the ranges of T_B and d are of course much broader and $\langle d_{act} \rangle$ is bracketed to indicate its larger uncertainty. By way of contrast, thermal fluctuation analysis of coercive force data using equation (3) yields a single weighted average figure $\langle d_{act} \rangle$, in which the weighting is done automatically and always in the same way.

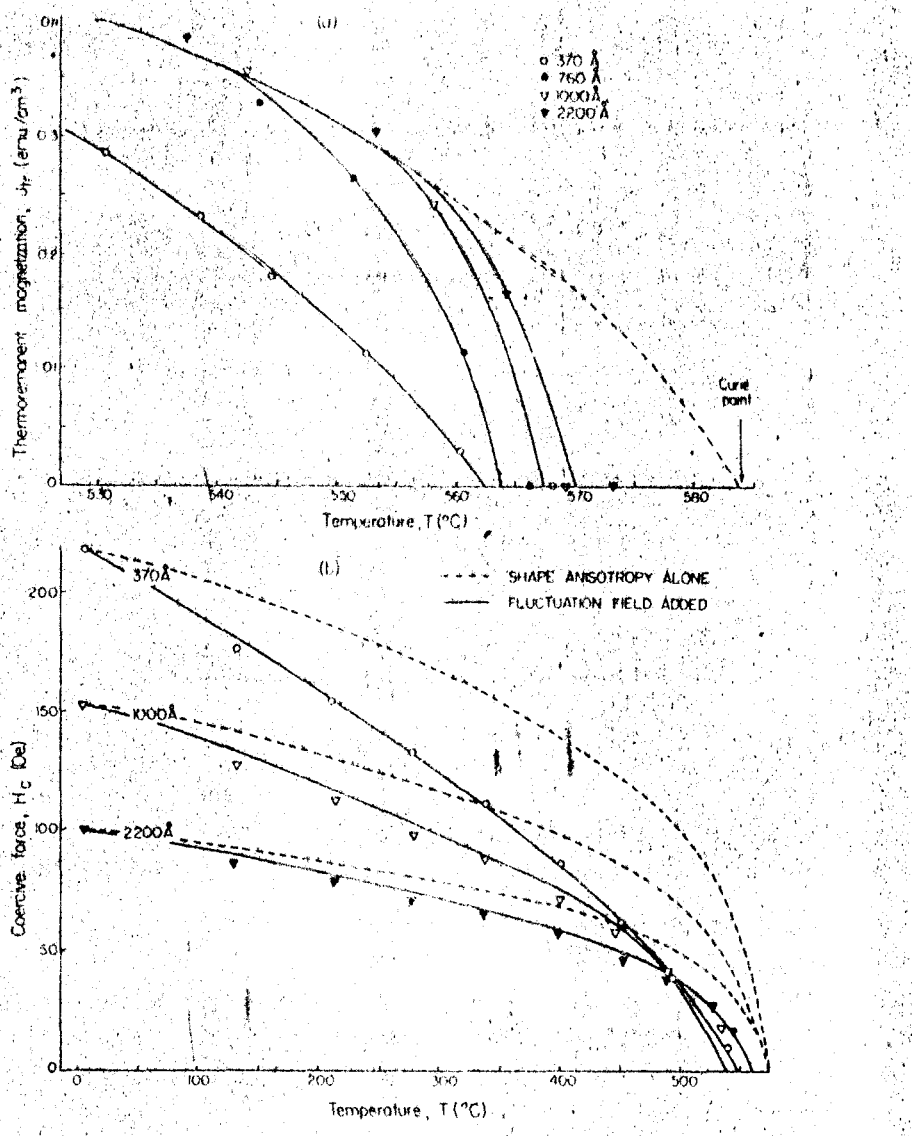

Figure 1. A comparison of blocking temperatures determined from TRM and from coercive force data. (a) Thermal demagnetization of 1-Oe TRM's — adapted from Dunlop (1973b). The measurements were made at high temperatures, not after cooling. Hence, the J_S–T curve of magnetite forms an envelope to the curves. The blocking temperatures are narrowly distributed, except in sample 4 (370 A). (b) Temperature dependence of bulk coercive force (experimental points) and attempted curve fits (after Dunlop 1976a). The data for sample 3 are omitted for clarity. Shape anisotropy (equation 1) fails to explain the data. Shape anisotropy plus an appropriate fluctuation field (equations (3) or (5)) fits the data quite well. The blocking temperatures in (a) and (b) are in agreement.

5 Thermal fluctuation analysis of high-temperature hysteresis data

Two parameters are commonly used as measures of the mean of the DC coercivity spectrum. One is the bulk coercive force, H_C, the reverse field that reduces the induced magnetization to zero following saturation. (Unfortunately H_C is generally used to symbolize both bulk coercive force of a sample and, as in equation (3), the coercive force or threshold field of a single particle. In what follows, the context will make clear which meaning is intended.) The

Table 1. Sizes of thermally activated regions in submicroscopic magnetite particles, as inferred from TRM unblocking and high-temperature hysteresis (Figs 1 and 2), compared with observed particle sizes.

Sample No.	Electron microscopy		T_B data		H_C data			H_R data		
	$\langle d \rangle$ (A)	σ_d (A)	$\langle T_B \rangle$ (°C)	$\langle d_{act} \rangle$ (A)	H_{C0} (Oe)	$\langle H_{K0} \rangle$ (Oe)	$\langle d_{act} \rangle$ (A)	H_{R0} (Oe)	$\langle H_{K0} \rangle$ (Oe)	$\langle d_{act} \rangle$ (A)
1	2200	420	566	1050	100	108	1610	266	305	1660
2	1000	290	560	900	153	175	1000	279	318	960
3	760	250	555	820	178	210	915	308	348	925
4	370	150	—	(550)	248	276	685	396	500	695

T_B data after Dunlop (1973b). The T_B spectrum of sample 4 is too broad for $\langle T_B \rangle$ to be meaningful. Cubic particles are assumed, i.e. $\langle d_{act} \rangle = \langle v_{act} \rangle^{1/3}$.

other is the remanent coercive force, H_R, the reverse field that reduces the remanence to zero following saturation, or the coercive force observed in a 'DC demagnetization' curve. H_R is a sort of median 'demagnetizing' field, in that it reverses one-half the saturation remanence J_{rs} of a sample. H_C is always less than H_R because less than one-half of J_{rs} is reversed, magnetization induced in the reverse direction by H_C making up the balance. H_C is therefore only indirectly related to average coercivity.

Dunlop (1976) reports H_C and H_R data for samples 1–4 measured at T_0 and at eight or nine elevated temperatures. The H_C results plotted in Fig. 1(b) are reproduced from his paper. Their most striking feature is the vanishing of coercive force 15–40°C below the Curie point, at the same blocking temperatures observed for TRM in Fig. 1(a). No thermal variation of H_K can explain this observation. The dashed curves in Fig. 1(b) indicate the thermal variation expected if H_C were due entirely to shape anisotropy ($H_C = H_K \propto J_S$, equations (1)).

Somewhat improved fits to the data are obtained using combinations of shape and crystalline anisotropy (curve fits not shown), but none can account for the data at both high and low temperatures. $H_K(T)$ due to magnetocrystalline anisotropy goes as a high power of $J_S(T)$ (equation (1)) and effectively vanishes well below the Curie point. Pure crystalline (perhaps also magnetoelastic) anisotropy could, in principle, explain the vanishing of coercive force below the Curie point. However, the lower temperature data require that H_K be predominantly due to shape anisotropy and so H_K, like the ferromagnetism itself, can vanish only at the Curie point.

Using H_K functions appropriate to domain rotation to fit data for larger than SD particles requires some justification. The $\langle d_{act} \rangle$ values derived from TRM data (Fig. 1(a) and Table 1) indicate activation of virtually the entire domain structure in samples 2–4. That is, rotation rather than wall motion must be occurring in these samples. In any case, $H_K(T)$ for MD particles (equations (1)) is likely intermediate in its dependence on $J_S(T)$ between shape and crystalline anisotropies, so that the present calculations provide upper and lower bounds.

5.1 FLUCTUATION FIELD FITS

When the effect of a fluctuation field is added to H_K, the vanishing of H_C below the Curie point is explained in a straightforward way. Also accounted for is the fact that H_C vanishes at lower temperatures in finer grains. (The only way of explaining this observed grain size dependence without invoking thermal agitation is to postulate two competing anisotropies, both going as high, but different, powers of J_S. One could perhaps appeal to the increasing role played by surface anisotropy in very fine particles, although there is no evidence of

surface pinning in the saturation magnetization. The $J_{sat}(T)$ curves of all the samples matched $J_S(T)$ for bulk magnetite very closely.)

The solid curves in Fig. 1(b) are the best fits of equation (3) to the data, assuming H_K arises entirely from shape anisotropy. This approach clearly does not give a unique solution, but it has the merit of simplicity. We are not asserting that crystalline anisotropy plays no role in our samples, but low-temperature fits left no doubt that its contribution was a secondary one. Within the precision of the present data, assuming mixed anisotropy greatly complicated the curve-fitting without much improving the match to the data at either high or low temperatures.

Since both sets of curves in Fig. 1(b) assume shape anisotropy for H_K, the difference between the curves is a measure of the fluctuation field, H_q, at any temperature. (The difference $H_K - H_C$ between the dashed and solid curves is not in fact *equal* to H_q because the H_K data have been multiplied by $J_S(290)/J_S(0)$ to produce a match at 290 K rather than 0 K). It is apparent that the fluctuation field, unlike other activation phenomena, is not confined to a threshold region of v or T, as is the case for example with the TRM unblocking of Fig. 1(a). H_q is substantial for all the particle sizes examined, even for 2200 Å particles whose volumes are 400 times v_s. (v_s for magnetite corresponds to a grain size of about 300 Å — Dunlop (1973c).) H_q is likewise substantial well below T_B, even at room temperature and below.

If H_K can be ascribed entirely or predominantly to shape anisotropy, H_K/J_S is temperature invariant and equation (3) can be written in the linear form

$$\frac{\langle H_C \rangle}{j_s} \approx \langle H_{K0} \rangle - \left[\frac{2k \ln(f_0 t)}{J_{S0}}\right]^{1/2} \langle H_{K0}^{1/2} \rangle \langle v_{act}^{-1/2} \rangle \frac{T^{1/2}}{j_s} \qquad (5)$$

where $j_s \equiv J_S(T)/J_{S0}$ and the subscript 0 refers to any convenient reference temperature, here 290 K. Fig. 2 shows the data plotted in this form. Both H_C and H_R are utilized as estimates of $\langle H_C \rangle$. As anticipated, the data deviate from straight lines at temperatures near T_B, but linearity is otherwise reasonably good. Sample 4, with the broadest size spectrum, displays the poorest linearity.

6 Activation volumes by thermal fluctuation analysis

The values of $\langle H_{K0} \rangle$ and $\langle d_{act} \rangle$ in Table 1 were calculated from the intercepts and slopes of the best-fitting lines through the data of Fig. 2, assuming $\langle H_{K0}^{1/2} \rangle \approx \langle H_{K0} \rangle^{1/2}$ and $\langle v_{act}^{-1/2} \rangle \approx \langle v_{act} \rangle^{-1/2}$. $J_{S0} = 485$ emu cm^{-3} and $\ln(f_0 t) = 23.6$ were assumed and $j_s(T)$ followed Pauthenet & Bochirol (1951).

Activation sizes calculated from H_C and from H_R data are practically identical. For these samples at least there is little to choose between H_C and H_R as estimates of mean coercivity. $\langle d_{act} \rangle$ from coercive force data is in each case slightly but significantly larger than $\langle d_{act} \rangle$ from blocking temperature data. The difference is probably due to the difference in the averaging processes used to arrive at $\langle d_{act} \rangle$. It may also be that the slopes in Fig. 2 are somewhat biased by data points in the blocking region. These points favour larger grains whose magnetization persists after smaller grains have been heated through their blocking temperatures.

$\langle d_{act} \rangle$ calculated by any method greatly exceeds $\langle d \rangle$ observed for sample 4. One reason is that $\langle d_{act} \rangle$ is a magnetically determined average. It excludes SPM particles, which comprise about 15 per cent by volume of the magnetite in sample 4, whereas $\langle d \rangle$ from electron micrographs or surface area measurements includes these finer particles. Even so, the $\langle d_{act} \rangle$

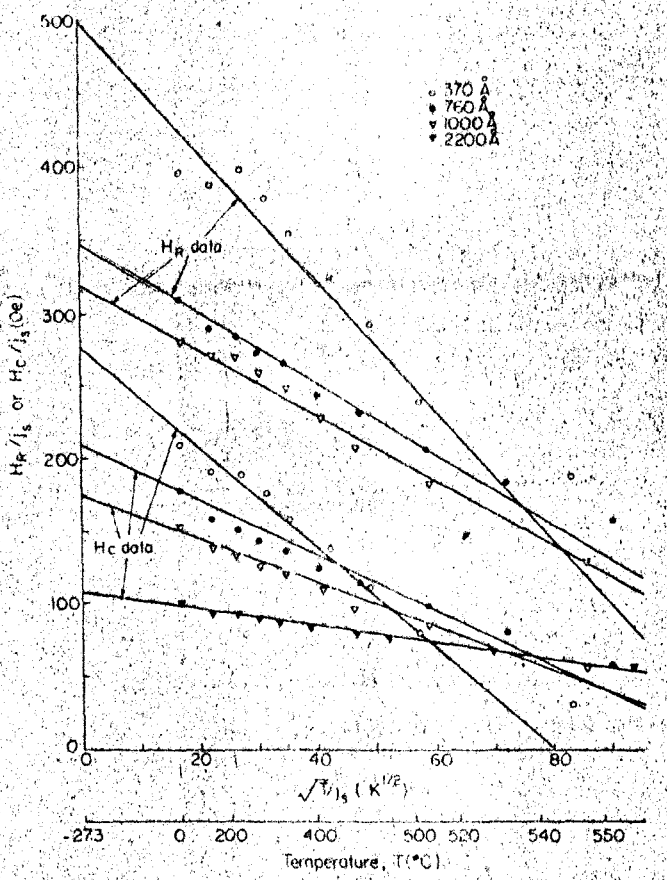

Figure 2. Thermal fluctuation analysis of remanent and ordinary coercive force data for samples 1–4, using equation (5). Linearity of the data confirms the predicted temperature dependence of the fluctuation field H_q. Intercepts of the lines are estimates of H_{K0}; slopes of the lines yield estimates of mean activation volume. H_R data for sample 1 are omitted for clarity.

estimates seem high, since the largest particles observed are only about 650 Å in size. Possibly neighbouring particles interact and to some extent act collectively. Craik & Isaac (1960) have noted such 'interaction domains' in fine-particle aggregates and Kneller & Wohlfarth (1966) discuss the possibility of thermal activation volumes greater than the volume of a single particle. Interactions due to particle clumping could of course occur in all the samples but would be especially severe in sample 4 because the fine grain size permits much smaller centre-to-centre separations.

In samples 2 and 3, practically the entire particle volume is activated as a unit. Nevertheless, there is no doubt that the magnetization in the remanent state is inhomogeneous. Domain structure just above the SD threshold must be a compromise between the uniform magnetization of SD particles and the broad domain, narrow wall conditions in large MD particles. Néel (1956) suggested that the transition to SD structure occurs when particles become too small to accommodate a domain wall. The calculations of Amar (1958) for iron and Butler & Banerjee (1975) for magnetite and titanomagnetite similarly support the notion that the domain wall fills a large fraction of particles just above SD size. Displacement of the wall then involves a small rotation of practically all the spins in the particle. That is, MD and SD magnetization processes merge into one. H_K would be close to that for

incoherent rotation (Frei *et al.* 1957) in particles just below SD size, so that $H_K \propto J_S$ as observed.

Only sample 1 has $\langle d_{act} \rangle$ significantly less than the observed mean grain size. Soffel (1971) has observed two-domain structure in high-Ti titanomagnetites not far above SD size and we will assume a similar structure is involved here. Two-domain particles have a permanent net moment perpendicular to the domain magnetizations due to the uncompensated moment $(2/\pi)J_S v_{wall}$ of the domain wall (Stacey & Banerjee 1974, p. 61). The reason for the disagreement (Table 1) between $\langle d_{act} \rangle$ estimated from H_C or H_R and that found from T_B is not known, but we will favour the former. Then v_{wall} is about 40 per cent of the mean particle volume and the wall moment is about 25 per cent that of an SD particle of equal size. Thus we would predict, for random orientations, $J_{rs}/J_S = 0.25(J_{rs}/J_S)_{SD} = 0.125$. The observed value is 0.113, so that the model of two-domain particles in which the domain wall moment is thermally activated seems reasonable.

7 The grain-size dependence of $\langle H_K \rangle$

If samples 1–4 contained SD particles with similar shape distributions, H_C, H_R and $\langle H_q \rangle$ would vary with the grain size but $\langle H_K \rangle$ would not. The size dependence of $\langle H_{K0} \rangle$ in Table 1 is further evidence that the particles in most of these samples are above SD size. Curling reversals in large SD particles, predominantly in rather elongated particles, impart a size dependence $H_K \propto d^{-2}$ (Frei *et al.* 1957), but the $\langle H_{K0} \rangle$ data in Table 1 vary as $d^{-0.6}$, a trend reminiscent of MD particles (Lubórsky 1961; Parry 1965). The value of the power-law index is diagnostic of the mechanism of coercivity (Stacey & Banerjee 1974, p. 67). An interpretation taking into account the probable domain structure of these particles is given elsewhere (Dunlop 1977, in preparation). We should note in passing, however, that a much smaller index (about 0.4) describes the size variation of H_C. Using raw coercive force data, as is the usual practice, can lead to a quite erroneous diagnosis. The size variation of H_K must always be separated from that of the fluctuation field, by the method of Fig. 2 for example.

8 The fluctuation field at T_0 and at T_B

Table 1 records a notable difference between observed room temperature coercive forces, H_{C0} and H_{R0}, and the corresponding microscopic coercive forces $\langle H_{K0} \rangle$ that would be observed in the absence of thermal fluctuations. The difference in each case is the fluctuation field $\langle H_q \rangle$ at T_0. $\langle H_{q0} \rangle$ is tabulated for the H_C data in Table 2. It varies from 7 per

Table 2. Estimates of the average thermal fluctuation field H_q at room temperature T_0 and at the blocking temperature T_B from thermal fluctuation analysis of coercive force data and from the TRM induction data of Dunlop (1973b). Symbols defined in text.

		Fluctuation analysis of H_C data				TRM induction data		
Sample No.	$\langle d \rangle$ (Å)	$\langle H_{K0} \rangle$ (Oe)	$\langle H_{q0} \rangle$ (Oe)	$\langle H_{qB} \rangle$* (Oe)	$\langle H_{qB} \rangle$† (Oe)	n	H_{break} (Oe)	$\langle H_{qB} \rangle$‡ (Oe)
1	2200	108	8	14	11	1.47	6.5	2.6
2	1000	175	22	37	46	1.79	5.8	1.7
3	760	210	32	54	76	1.82	7.8	2.2
4	370	276	58	98	(100)	1.97	11.0	2.8

* $\langle H_{qB} \rangle = \langle H_{q0} \rangle (T_B/T_0)$ (text, equation (6))

† $\langle H_{qB} \rangle = [2kT_B \ln (f_0 t)/J_{S0}]^{1/2} \langle H_{K0}^{1/2} \rangle \langle v_{obs}^{-1/2} \rangle$ (text, equation (7)).

‡ $\langle H_{qB} \rangle = [(n-1)^{n-1}/n^n] H_{break}$ (text, equation (8)).

cent of $\langle H_{K0}\rangle$ in 2200 Å particles to > 20 per cent of $\langle H_{K0}\rangle$ in 370 Å particles. Considering that 2200 Å particles have volumes more than two orders of magnitude larger than the SPM volume v_s, this is a remarkable manifestation of thermal fluctuations. Levi (1974), on the other hand, is able to account for the temperature dependence of median demagnetizing field in magnetites with a mean grain size 2100 Å without appealing to thermal agitation. He finds $H_C(T) \propto J_S^{2.5}(T)$, a result that we find, in a later section, holds for much larger grains (1–5 μm in size.)

The average fluctuation field $\langle H_{qB}\rangle$ at the blocking temperature can be calculated from the data of Fig. 2 and Table 1 in two quasi-independent ways. Using the intercepts $\langle H_{K0}\rangle$ from Fig. 2, we can extrapolate $\langle H_{q0}\rangle$, according to equation (3) or (5)

$$\langle H_{qB}\rangle = \langle H_{q0}\rangle (T_B/T_0)^{1/2} = (\langle H_{K0}\rangle - H_{C0})(T_B/T_0)^{1/2}. \tag{6}$$

Alternatively, by direct calculation, using the same equations and observed average grain sizes,

$$\langle H_{qB}\rangle = [2kT_B \ln(f_0 t)/J_{S0}]^{1/2} \langle H_{K0}^{1/2}\rangle \langle v_{obs}^{-1/2}\rangle. \tag{7}$$

Again the approximations $\langle H_{K0}^{1/2}\rangle \approx \langle H_{K0}\rangle^{1/2}$, $\langle v_{obs}^{-1/2}\rangle \approx \langle v_{obs}\rangle^{-1/2}$ were made. Shape anisotropy was assumed in both calculations. The second calculation is very uncertain for sample 4 because the value $\langle v_{obs}\rangle$ to be used is uncertain. The comparison estimates of $\langle H_{qB}\rangle$ agree about as well as $\langle d_{act}\rangle$ and $\langle d_{obs}\rangle$ values agree in Table 1 (the comparisons are, in fact, analogous).

$\langle H_{qB}\rangle$ enters the Néel (1955) theory of TRM in small MD grains. For small values of the applied field H, thermal fluctuations dominate the blocking process and TRM intensity should be proportional to H. At high fields, wall opposition is dominant and TRM $\propto H^{1-1/n}$, where n is the power-law index in equation (1). The break-point between these dependences has been observed experimentally (Dunlop 1973b; Day 1973). Theoretically the break-point field H_{break} is related to $\langle H_{qB}\rangle$ by the equation (Dunlop & Waddington 1975)

$$\langle H_{qB}\rangle = [(n-1)^{n-1}/n^n] H_{break}. \tag{8}$$

Using values of n and H_{break} from Dunlop (1973b, Fig. 6), we arrive at values of only 2–3 Oe for $\langle H_{qB}\rangle$ in all the samples. While granting that the n values may be somewhat high, since they were determined from the raw $H_C(T)$ data and not from $H_K(T)$, $\langle H_{qB}\rangle$ certainly cannot exceed H_{break}. A residual difference of an order of magnitude at least remains between $\langle H_{qB}\rangle$ values estimated from coercive force data and $\langle H_{qB}\rangle$ values inferred from TRM induction.

We cannot explain this discrepancy by appealing to the dependence of T_B itself on applied field (Schmidt 1976). The observed blocking temperatures of low-field TRM (Table 1) yield $\langle d_{act}\rangle$ estimates in quite reasonable accord with $\langle d_{act}\rangle$ values determined by fluctuation analysis of large-field hysteresis data. That is to say, our picture of thermal fluctuations does predict about the right (i.e. the observed) blocking temperatures for TRM. Indeed, the $\langle H_{qB}\rangle$ values in the last column of Table 2 can only be reconciled with $\langle H_{q0}\rangle$ observations by invoking blocking temperatures *below* room temperature!

A further point is that the $\langle H_{qB}\rangle$ values from equation (8) have essentially no grain size dependence, whereas equations (3), (4), (5) and (7) predict a strong size dependence, which is unmistakably manifested in the slopes in Fig. 2. (The fact that T_B decreases as v decreases is quite insufficient to offset this size dependence.)

There seem to be three possibilities.

(1) The Néel (1955) wall displacement theory is deficient.

(2) The Néel (1955) theory does describe normal MD grains, but not grains just above SD size. (However, sample 1 contains two-domain grains like those modelled by Néel and the discrepancy here, although less than that for samples 2–4, remains significant.)

(3) The Néel (1955) theory describes MD grains, large or small, but the break-point observed experimentally at intermediate fields is not appropriate to equation (8). (Conceivably, break-points observed by Day (1973) and Dunlop & Waddington (1975) around 100 Oe are the break-point envisaged in Néel's theory.)

9 A calculation of superparamagnetic threshold size

The dependence of $\langle H_q \rangle$ on grain size is given quantitatively by equation (4), which can be rewritten

$$\langle H_q \rangle / \langle H_K \rangle = (\langle H_K \rangle - H_C)/\langle H_K \rangle = (v_s/\langle v_{act} \rangle)^{1/2} \tag{9}$$

Equation (9) also provides a means of experimentally determining the SPM threshold size d_s at room temperature (or any temperature for that matter) by non-threshold measurements. Fig. 3 is a test of equation (9), using $\langle H_{q0} \rangle$, $\langle H_{K0} \rangle$ and $\langle v_{act} \rangle$ data from Tables 1 and 2. The data are fit reasonably well by a straight line whose slope yields an SPM size d_s of 250 Å. This estimate is within the uncertainty of the figures (290–360) ± 50 Å obtained by an independent experimental method (Dunlop 1973c).

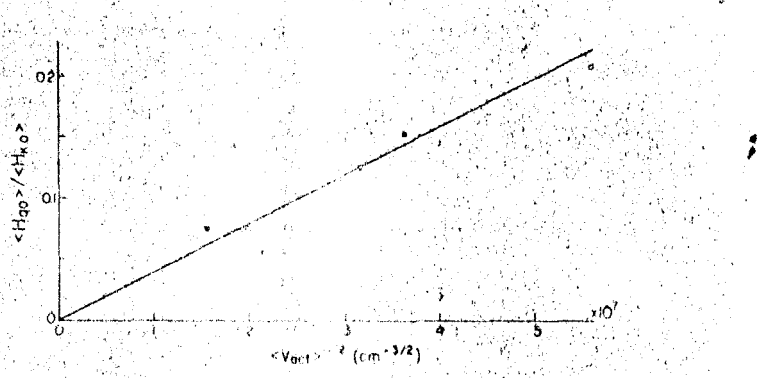

Figure 3. A test of the predicted (equations (4) and (9)) grain size dependence of the fluctuation field. The slope of the graph yields a value for the superparamagnetic threshold size d_s in magnetite of approximately 250 Å.

The uncertainty in the present estimate, due to uncertainty in the slope in Fig. 3, is $(^{+10}_{-25}$ Å), much less that the uncertainty with any previous method of determining d_s. The great advantage of the present method is that only H_C and T need be measured. $\langle v_{act} \rangle$ is a calculated quantity. Grain size determinations, which are notoriously imprecise, need not be made. On the other hand, the method is indirect, in that it relies on the Néel (1949) activation equation.

10 High-temperature AF demagnetization

High-temperature AF demagnetization makes it possible to refine the studies of the previous sections by examining separately the thermal evolution of different parts of the coercivity spectrum. Several previous studies (Larson *et al.* 1969; Dunlop & West 1969; Bina 1971; Levi 1974) have investigated in this way the relationship between average coercive force and the spectrum of coercivities. The experiment is not an easy one, particularly at temperatures

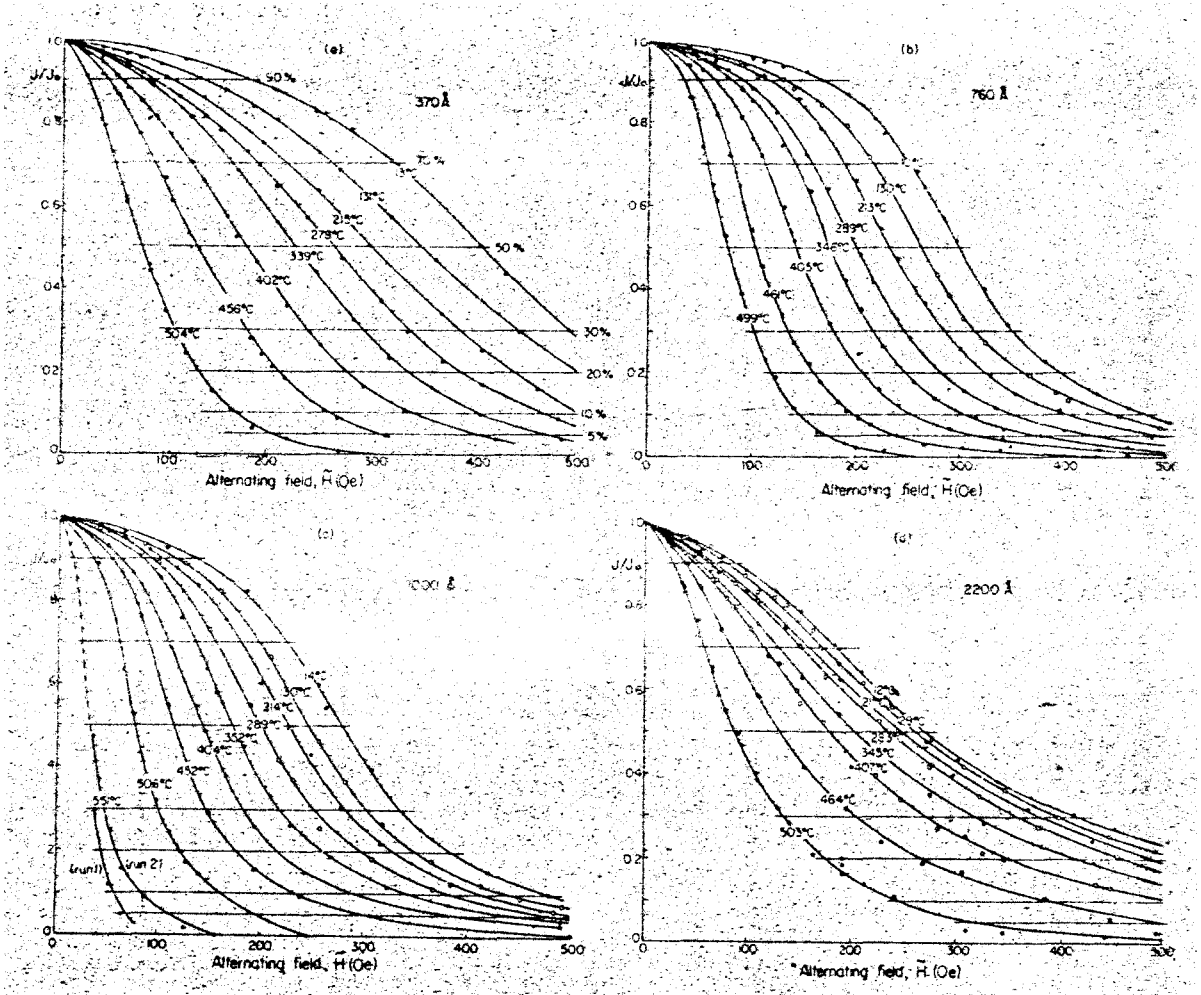

Figure 4. Alternating-field demagnetization of the saturation remanence of samples 1–4, measured at high temperatures. Horizontal lines denote the seven remanence fractions whose average coercivities are analysed separately in the text.

within 100°C or so of the Curie point, where temperature non-uniformity and drift must be held to a few degrees. (Note, for example, the replicate curves, both nominally measured at 551°C in Fig. 4(c).) Particularly high precision and repeatability were sought in the present work, since sometimes small differences between demagnetization curves were to be analysed in the same manner as the bulk coercive force data of the previous section.

The results are shown in Fig. 4. In each case, a saturation remanence (in 2.3 kOe) was induced and progressively AF demagnetized at the temperature shown. Demagnetization of small-field TRM or ARM (anhysteretic remanent magnetization) gives equivalent but noisier results and makes for less accurate differencing of curves. With occasional exceptions, e.g. the low-field data at 130°C in Fig. 4(b), the results are of high precision, so far as one can judge by the smoothness of the curves. Seven fractions of the coercivity spectrum were analysed. As indicated in Fig. 4, these are at fixed remanence levels of 90, 70, 50, 30, 20, 10 and 5 per cent of J_{rs}, ensuring, as far as possible, that the same particles are being measured at different temperatures.

11 Activation volumes by fluctuation analysis of AF data

Fig. 5 shows the results of an analysis like that of Fig. 2, again assuming $H_K \propto J_S$ and using the AF demagnetizing fields H_C of the various fractions as measures of H_C in equation (5). Features that were lumped together and averaged out in Fig. 2 are resolved in Fig. 5. The non-ideality of sample 4 can no longer be glossed over. Its distribution of blocking temperatures means that some remanence is lost between low and high temperatures, so that coercivity fractions selected on the basis of their remanence fraction are not comparable at different temperatures.

The reasons for the failure of the theory to fit the sample 1 results is not known. In the AF data, Fig. 4(d), and in Fig. 5(d), there is a suggestion of two types of moments with different properties. The hardest fractions (10 and 5 per cent) actually have higher coercivities than the corresponding fractions for smaller particles, and they seem to have a distinctive thermal dependence as well. Perhaps we are seeing resolved here the characteristics of PSD moments of two quite different types, one of which is absent in grains too small to have well-defined two-domain structure.

Samples 2 and 3 appear to have linear trends for all coercivity fractions, with considerable scatter that was presumably averaged out in Fig. 2. Using H_{K0} for each fraction from the intercepts in Fig. 5(b) and (c), the slopes were analysed to give the values of $\langle d_{act} \rangle$ listed in Table 3. The results for the 10 and 5 per cent fractions are rather uncertain, but the general agreement in $\langle d_{act} \rangle$ values for the various fractions is reassuring. The mean values for $\langle d_{act} \rangle$, averaging all the fractions, actually agree better with the observed mean grain sizes than did the bulk coercivity results of Table 1. This close agreement may well be fortuitous. It is interesting that $\langle d_{act} \rangle$ tends to be smaller for harder (i.e. more elongated or irregular) particles. One of our initial assumptions, that $f(v, H_K) = \phi(v)\,\psi(H_K)$, is therefore violated, but not seriously enough to invalidate the approach of Fig. 2.

12 Dependence of the fluctuation field on H_K

The slopes in Fig. 5(b) and (c) increase with increasing coercivity. This is an expected effect, since H_q depends on H_K (equation (3)). In fact, according to equation (5), the slope $d(H_C/J_S)/d(T^{1/2}/J_S)$ is proportional to $(H_{K0})^{1/2}$. In effect, we have already tested this prediction. It was implicit in the calculations that led to the results in Table 3. Fig. 6 shows an

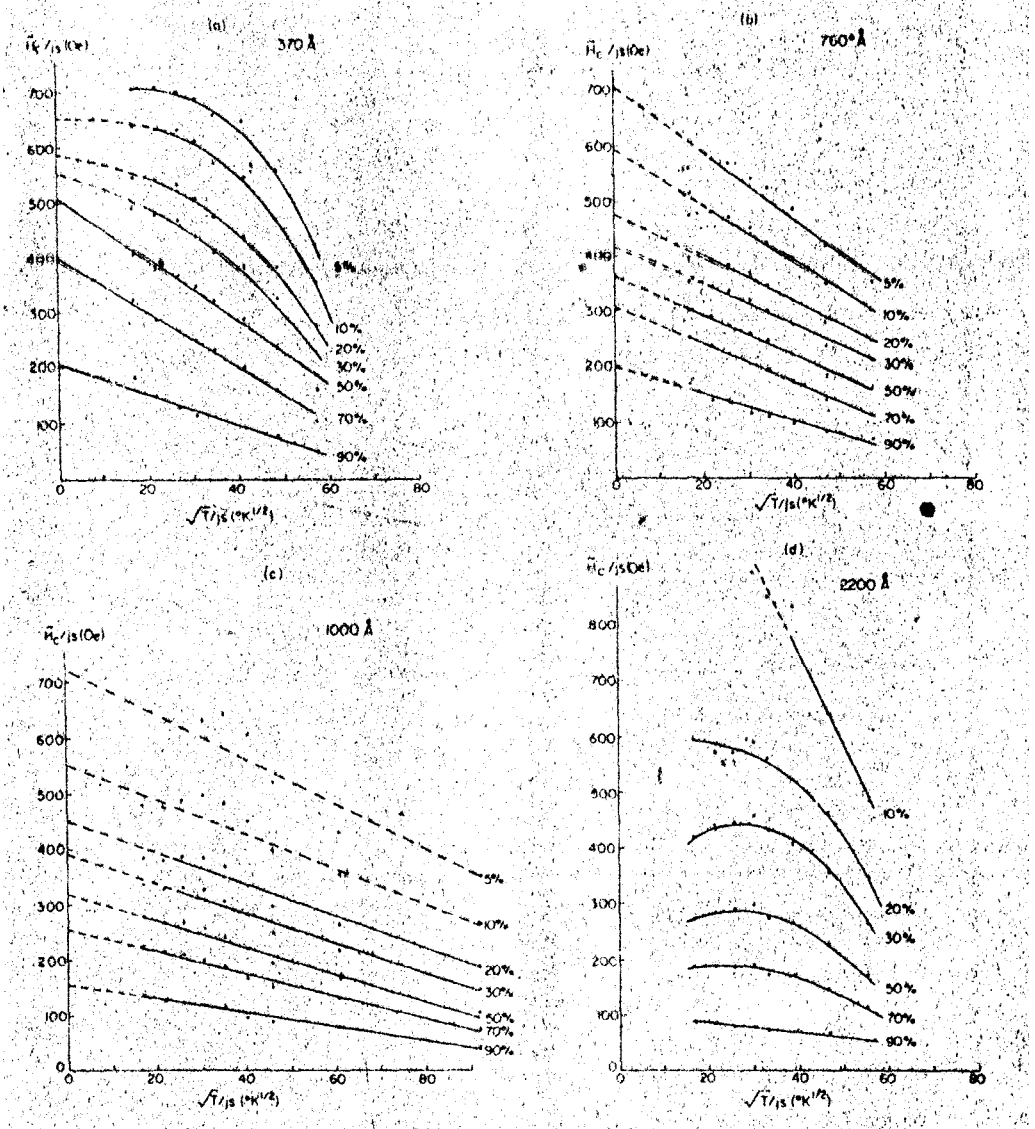

Figure 5. Thermal fluctuation analysis, in the manner of Fig. 2, of the high-temperature AF coercivities of seven different remanence fractions of samples 1–4 (data from Fig. 4). 'Non-ideal' behaviour (i.e. non-linearity) may reflect the influence of crystalline anisotropy or the experimental difficulty of measuring the tail of the AF demagnetization curve with sufficient accuracy at high temperature.

Table 3. Activation volumes calculated for separated coercivity fractions from the high-temperature AF demagnetization data (Fig. 5).

	(d_{act}) for each coercivity fraction (Å)								
Sample No.	90 per cent	70 per cent	50 per cent	30 per cent	20 per cent	10 per cent	5 per cent	Mean* (d_{act}) (Å)	Observed (d) (Å)
2	1090	940	895	895	900	910	840	920	1000
3	780	705	735	755	735	675	645	720	760

* Arithmetic mean of (d_{act}) values of the seven fractions.

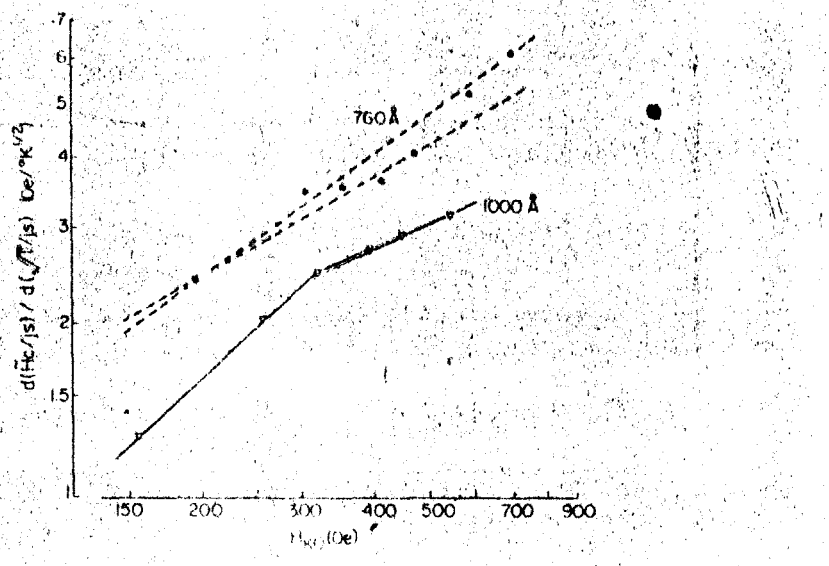

Figure 6. A test of the predicted dependence of the fluctuation field on microscopic coercive force, H_{K0}, for the two samples (2 and 3) that showed 'ideal' behaviour in Fig. 5. Note the log–log scale. The harder fractions of sample 2 exhibit a slope close to the expected 1/2, while the softer fractions define a slope closer to 1, the value expected for magnetocrystalline anisotropy, without shape anisotropy or a fluctuation field. The data for sample 3 are too scattered to draw any conclusions.

explicit test, a bilogarithmic plot of slope versus intercept field H_{K0} for the data of Fig. 5(b) and (c).

The results are rather scattered for sample 3, but the slope lies between the expected 0.5 and an upper limit of 0.7. The softest fractions of sample 2 yield a slope of about 0.9, the harder fractions a slope near 0.5. There is a simple explanation for slopes > 0.5. Equation (5) assumes shape anisotropy, so that the only H_K dependence enters via the $H_K^{1/2}$ variation of H_q. If, however, crystalline anisotropy also contributes to H_K, both terms on the right-hand side of (5) are temperature dependent. The crystalline anisotropy is, of course, proportional to H_{K0}, not $(H_{K0})^{1/2}$. Such a contribution is most likely in the least elongated particles, i.e. the soft fractions, as the results for sample 2 seem to attest.

13 Coercivity fractions and bulk coercivity compared

It is instructive to plot the normalized temperature dependence of the $\tilde{H}_C$ data as in Fig. 7. The tabulated values illustrate the well-known fact that the bulk coercive force is numerically a poor indicator of the average of the coercive force spectrum. As explained earlier, H_C by its very nature is always less than the median value of the $\tilde{H}_C$ spectrum. It is also well known that H_C is biased towards softer fractions (particularly SPM particles) because these fractions have high susceptibility and low remanence. Fig. 7 illustrates just how strong that bias can be, even in samples with fairly narrow spreads of sizes and coercivities.

The temperature dependence of H_C is quite clearly *not* the average temperature dependence of the various fractions. Our choice of fractions does not of course cover the remanence spectrum uniformly (it would if the 20 and 5 per cent fractions were eliminated). Nevertheless, it is clear that $H_C(T)$ strongly resembles $\tilde{H}_C(T)$ of the softest fractions. In sample 2, we even have the anomalous situation where H_C decreases more rapidly than even the 90 per cent fraction, and does not in any sense constitute an average. Although the underlying cause remains obscure, the results of Fig. 7 explain why the $\langle d_{act} \rangle$ estimates of Fig. 1, based

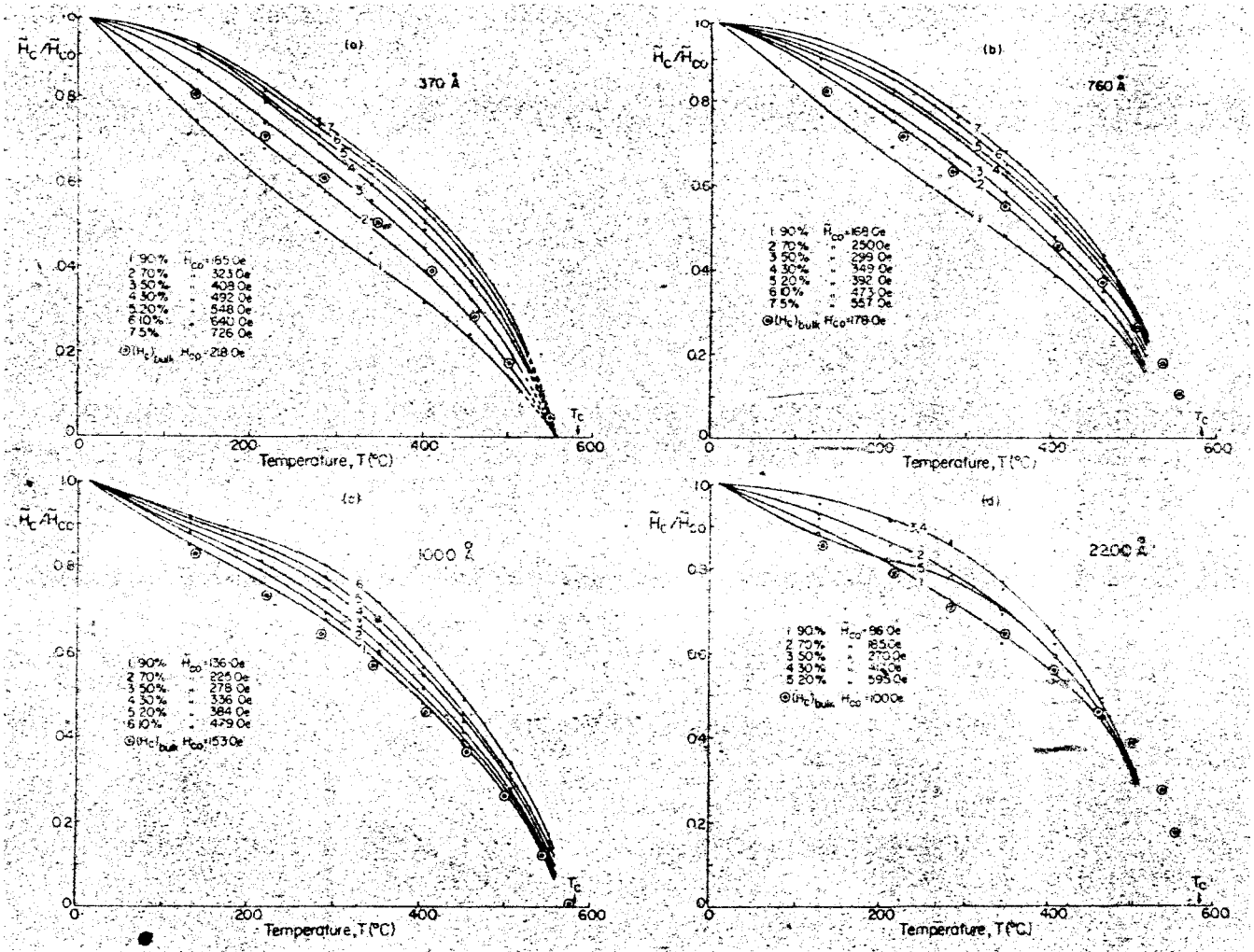

Figure 7. A comparison of the temperature variations of AF coercivity of seven separated fractions of the coercive force spectrum with the temperature variation of bulk coercive force. Ordinary coercive force is a poor spectral average. In magnitude and temperature dependence, it matches the softest 20–30 per cent of the spectrum. However, the remanent coercive force H_R (data not shown) is closely representative of the median demagnetizing field of the spectrum. The harder fractions of sample I (2200 A) are unexpectedly hard and have an unusual temperature dependence. They may reflect the onset of a new type of magnetic moment in two-domain grains with well-developed walls.

on bulk coercive forces, match the values calculated for the softest (90 and 70 per cent) $\tilde{H}_C$ fractions in Table 3 and not the mean of all $\tilde{H}_C$ fractions.

Fig. 7 also allows us to check the assumption of shape anisotropy. $\tilde{H}_C(T)$ for the harder fractions does indeed resemble $J_S(T)$, but for the softer fractions, $\tilde{H}_C$ varies as increasingly higher powers of J_S. That is, there is an increasing contribution due to magnetocrystalline anisotropy in more nearly equant particles, just as one would expect. The results for the harder fractions (20, 10 and 5 per cent) in sample 1 are anomalous. The 10 and 5 per cent fractions have temperature variations too irregular to join with a smooth curve. As mentioned before, these fractions seem to behave in a unique manner and may reflect a mechanism of PSD behaviour not present in smaller particles.

14 Thermal fluctuation analysis of large PSD particles

The published high-temperature hysteresis and AF demagnetization results of Bina (1971) lend themselves to a thermal-fluctuation analysis. Moreover, the experiments were carried out on magnetite that is unusually pure, strain-free and narrowly sized (1–5 μm) for the micron size range. The object of the analysis was to determine, if possible, the nature of PSD moments in fairly large particles not too far below the PSD threshold size (≈ 15 μm).

Either the moments are related to entire domain walls (wall moment or Barkhausen discreteness mechanisms), or they arise from regions of approximately SD size (surface moments, bending of segments of a domain wall around individual defects). These alternatives have very different activation volumes. For a 2-μm particle, say, even if the Barkhausen jump is only 10 Å (approximately the unit cell dimension), v_{act} is about 30 times v_{act} for a SD particle of critical size (500 Å). This contrast has been remarked upon by Dunlop (1973a) in connection with the magnetic viscosity of MD particles. Paradoxically, the VRM of MD material should be much less than that of SD material because of the large v_{act} of domain walls, yet the common experience in paleomagnetic studies is that soft (low-H_C) rocks with MD character are frequently very viscous.

14.1 BULK COERCIVE FORCE ANALYSIS

Fig. 8 is a plot of Bina's bulk coercive force data, in the manner of Figs 2 and 5. H_C is in normalized form: $h_c = H_C(T)/H_{C0}$. The convex downward curve in Fig. 8 is reminiscent of a

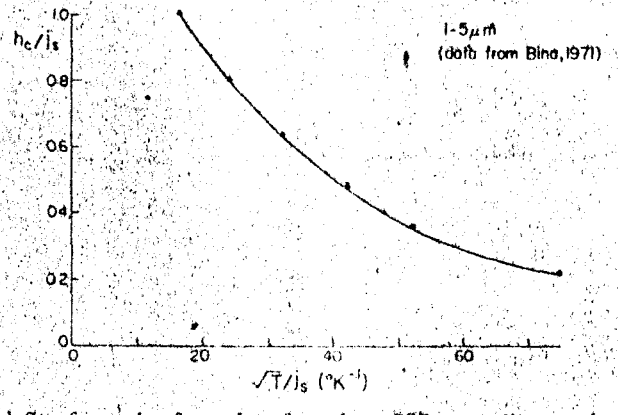

Figure 8. Attempted fit of coercive force data for a large PSD magnetite sample to equation (5). The simple thermal fluctuation analysis fails. PSD moments in these grains are either too large to be thermally activated to any appreciable extent, or else they have a very broad distribution of activation volumes.

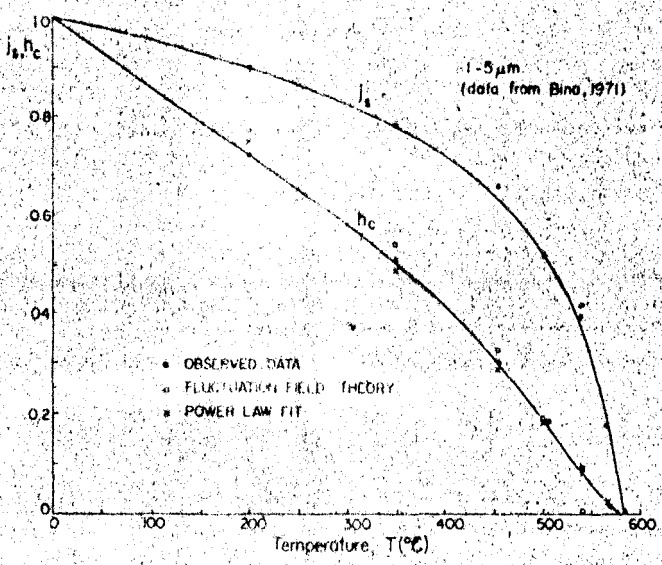

Figure 9. Normalized saturation magnetization and bulk coercive force data for the large PSD sample. Opposition to domain wall motion, with a power law dependence on temperature, fits the h_c data better than thermal activation of small PSD moments.

result reported by Dunlop (1976) for an SD sample which did not fit equation (5), either because its grain size spectrum was too broad or because H_K was not proportional to J_S (the particles were essentially equant and crystalline anisotropy was known to be important). One or both of these effects is reflected also in Fig. 8.

An average fit to the data indicates $\langle H_{K0} \rangle = 1.25 \langle H_{C0} \rangle$. Using the median demagnetizing field $\tilde{H}_{1/2}$ to approximate $\langle H_{C0} \rangle$ (in view of the conclusions of the previous section that bulk coercive force constitutes a poor numerical average), we have $\langle H_{K0} \rangle = 345$ Oe. Using this value throughout, $\langle d_{act} \rangle = 550$ Å for the low-temperature data and $\langle d_{act} \rangle = 850$ Å for the high-temperature data. (Cubic regions were assumed, but equivalent sphere diameters could equally well be quoted.) Remembering the powerful averaging effect evidenced by Fig. 2 as compared with Fig. 5 when fairly narrow size distributions are involved, we recognize that the present spectrum is very much broader than 550–850 Å. These are merely slightly displaced average figures in a spectrum so broad that the same average does not describe both low- and high-temperature results. The poor fit obtained with a single $\langle v_{act} \rangle$ of 650 Å at all temperatures is shown in Fig. 9.

When we consider the other possible explanation of the results, that H_K is not proportional to J_S but to some power of J_S, we find a close fit to the data at all temperatures if $h_c = j_s^{2.5 \pm 0.1(5)}$.

This mechanism would imply that thermal activation is insignificant, presumably because whole domain walls are involved and $\langle v_{act} \rangle$ is so large that in equation (2) $H_q < H_K$ even at high temperatures, and that n in equation (1) is about 2.5. Since n is controlled mainly by magnetostriction, which is known to have a considerably weaker temperature dependence than crystalline anisotropy (Syono 1965; Klapel & Shive 1974), this figure is not unreasonable.

14.2 AF DEMAGNETIZATION ANALYSIS

Since Fig. 8 does not give a linear result, Bina's AF demagnetization curves cannot be analysed in the manner of Figs 5 and 6. Instead we will analyse $\Delta \tilde{H}_C$ between each of Bina's

four high-temperature curves and the room-temperature curve, rather in the manner of Kneller & Wohlfarth (1966) and Gustard & Köster (1967). However, where these workers examined only two temperatures, the highest being 80°C, we examine five temperatures from 20 to 400°C for the same seven coercivity fractions studied in the last section.

Since we are attempting to distinguish between two alternatives, (1) thermal fluctuations of small regions with different average sizes at different temperatures, and (2) domain-wall pinning in which thermal activation plays a minor role, it is useful to recast equation (3) into two alternative forms:

$$\log \Delta(\tilde{H}_C/j_s) = \tfrac{1}{2} \log H_{K0} + \log [(\text{const}/\langle v_{act} \rangle^{1/2})\, \Delta(T^{1/2}/j_s)] \tag{10a}$$

$$\log \Delta(\tilde{H}_C/j_s) = \log H_{K0} + \log \Delta(j_s^{n-1}) \tag{10b}$$

Equation (10a) is appropriate to model 1, provided $H_K \propto J_S$. Graphs of $\log \Delta(\tilde{H}_C/j_s)$ versus $\log H_{K0}$ for different temperature intervals may have different intercepts, because of different $\langle v_{act} \rangle$, but they should all have slope ½. The same plots, if model 2 (equation (10b)) is appropriate, should have a slope of 1.

These ideas are tested in Fig. 10, which is a log–log plot. The linearity is not impressive, but the slopes seem to increase with temperature, from 0.45 for the 130–20°C curve differencing, to 0.57 for 210–20°C and 300–20°C, to 0.75 for 400–20°C. The uncertainties are large. For example, 0.45 is not a reasonable slope, since no model can generate a slope < 0.5. On the whole, the results would seem to favour thermal fluctuations of small regions at temperatures just above T_0, with domain wall effects becoming more prominent at high temperature. There is no reason to expect such a trend, and so the results of Fig. 10 are probably not diagnostic.

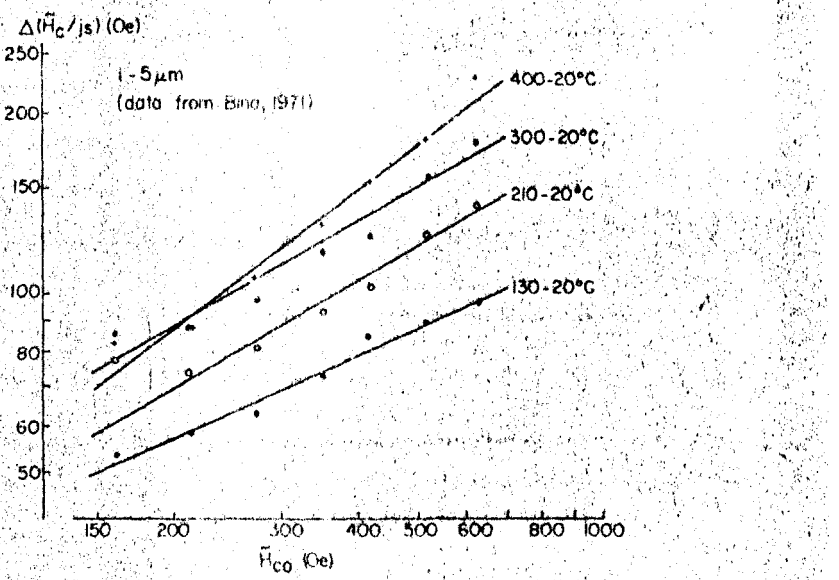

Figure 10. Test of the mechanism of high-temperature coercive force in large PSD grains of magnetite. Pairs of high-temperature AF demagnetization curves – for data, see Bina (1971) – were differenced at the same seven remanence levels used with samples 1–4 to test the predictions of equation (10). Note the log–log scale. As with the analogous method of Fig. 6, a slope of 1/2 indicates thermal activation of $\ll$1-μm size moments while a slope of 1 indicates negligible influence of thermal fluctuations on coercivity. The slopes here are mostly nearer 1/2 than 1, but are not considered definitive.

15 Discussion

15.1 AVERAGE COERCIVE FORCE – THE BEST ESTIMATE

The bulk coercive force of a mixture of ferromagnetic grains, according to Bean (1955), is less than the weighted average of the individual coercive forces. Just how strong the bias towards the soft end of the coercive force spectrum can be is illustrated by Table 4 and Fig. 7. H_{C0} of each sample is only slightly greater than the AF necessary to erase 10 per cent of the saturation remanence. In other words, H_{C0} is roughly equivalent to the average coercivity $\bar{H}_{C0}$ of the softest 20–30 per cent of the coercivity spectrum. This same equivalence applies at high temperatures, to judge by the temperature variations of H_C and $\bar{H}_C$ shown in Fig. 7.

Table 4. A comparison of room-temperature bulk coercive force H_C, remanent coercive force H_R and AF demagnetizing fields $\tilde{H}$ required to destroy 10 and 50 per cent of the saturation remanence of samples 1–4 (370–2200 A mean grain sizes).

Sample No.	H_{C0} (Oe)	$(\tilde{H}_{C0})_{10\text{ per cent}}$ (Oe)	H_{R0} (Oe)	$(\tilde{H}_{C0})_{50\text{ per cent}}$ (Oe)
1	100	86	266	270
2	153	136	279	278
3	178	168	308	299
4	218	185	396	408

H_{C0} is entirely unrepresentative of the median demagnetizing field $\tilde{H}_{1/2}$ (i.e. $(\tilde{H}_{C0})_{50\text{ per cent}}$). The remanent coercive force, H_{R0}, however, is *very* nearly equal to $\tilde{H}_{1/2}$. Furthermore, the temperature dependence of H_R, although it is not shown in Fig. 7, lies above that of H_C and resembles that of the median (40–60 per cent) fraction of the saturation remanence. H_R is in all respects a better estimate of average coercive force than H_C.

15.2 THE NÉEL THEORY OF THERMAL FLUCTUATIONS TESTED

Samples 1–4, although they contain grains that are for the most part above SD size, seem to change their magnetization by domain rotation in the SD manner. If this is the case, even though the volume affected by thermal agitation may be less than the total particle volume, the predicted dependence of Néel's fluctuation field on temperature, on microscopic coercive force, and on grain size (equations (3), (4) and (5)) can be tested.

The predicted (equation (5)) temperature dependence of H_q was followed by the harder fractions of the coercive force spectrum (Fig. 5) and by the average over all fractions (Figs 1 and 2), despite the fact that the average represented by H_C favours the soft fractions. Activation volumes inferred from the slopes in Figs 2 and 5 were reasonable (Tables 1 and 3). Magnetocrystalline anisotropy is the probable source of deviation from theoretical predictions in the soft fractions.

The predicted (equation (4)) size dependence of H_q (averaged over all fractions) was followed (Fig. 3). The superparamagnetic threshold size inferred from the slope of Fig. 3 agrees closely with independent experimental and theoretical estimates.

The predicted (equation (5)) H_K dependence of H_q was approximately verified for samples 2 and 3 (Fig. 6) by examining seven different fractions of the coercive force spectrum. Such a test can only be made if the data for each fraction display the expected temperature dependence. A *minimum* test requires coercive force data at *two* different

temperatures (e.g. Kneller & Wohlfarth 1966) for all the fractions, but a test of this sort for 1–5 μm magnetite grains (Fig. 10) gave ambiguous results. Nevertheless such a test is worth attempting because it is capable, in principle, of distinguishing between crystalline anisotropy and thermal fluctuations as the dominant mechanism in the decrease of coercive force upon heating and the blocking of TRM upon cooling (*cf.* equation (10)).

15.3 THE NATURE OF PSD MOMENTS

The superparamagnetic threshold size d_s obtained by extrapolation from the properties of grains mostly above SD size (Fig. 3) is (250^{+10}_{-25}) Å. This figure is indistinguishable from an experimental estimate of $d_s = (290 \pm 60) \pm 50$ Å (Dunlop 1973c) based entirely on SD measurements. By inference, even the largest PSD grains in the present study, with activation volumes two orders of magnitude larger than the volume of a particle of critical SPM size, behave in a manner reminiscent of SD particles.

The activation volumes of the grains in sample 1 are, however, substantially less than the total volume of each grain (Table 1). A two-domain structure is hypothesized, the domain wall itself carrying an uncompensated magnetic moment. The Barkhausen discreteness effect (Stacey 1963; Stacey & Banerjee 1974) may contribute to the moment, but the magnetization does *not* change by wall displacement. Wall displacement in MD grains, large or small, is limited by the internal demagnetizing field created when the wall moves from a central position, whereas sample 1, like samples 2–4, behaves in an SD-like manner. Wall moments in small PSD grains, whether intrinsic or due to non-central location of the wall, apparently respond to a field by rotating, presumably in the plane of the wall.

If the grains are less than about 1000 Å in size, essentially the entire domain structure rotates as a unit (Table 1, $\langle d_{act} \rangle$ results for samples 2 and 3). The domain wall and its neighbouring domains are tightly coupled in this case. Since the wall's behaviour determines the behaviour of the domains, it is reasonable to suppose the wall fills much of the grain.

The Néel (1955) theory of TRM, based on wall displacements in MD grains, predicts values of H_q at the blocking temperature that are an order of magnitude or more less than $H_q(T_B)$ inferred from fluctuation analysis and that lack the expected dependence on grain size. Although a wall-displacement model may fit the behaviour of larger MD grains, we believe domain rotation is dominant in 0.25 μm and smaller magnetite grains.

PSD behaviour is evidenced in the hysteresis and TRM of > 1 μm magnetite grains (Parry 1965; Day 1973; Bailey 1975). Fluctuation analysis of 1–5 μm magnetite grains failed to elucidate the nature of the PSD moments in these grains, however. In fact, the data of Figs 9 and 10 can be accounted for adequately by attributing the decrease in coercive forces upon heating entirely to the temperature variation of intrinsic opposition to wall motion. Thermal activation of domain walls may be occurring, but the large activation volumes involved result in a fluctuation field too small to be resolved with certainty. PSD moments with a broad distribution of submicron sizes would also explain the data, but their presence cannot be demonstrated unambiguously.

We arrive, therefore, at a curious paradox. The *grain size* dependence of H_C below ≈ 15 μm (Parry 1965) suggests that PSD moments make an important contribution to hysteresis, just as they undoubtedly do to low-field TRM. The *temperature* dependence of H_C and of the coercive force spectrum, however, can be accounted for if hysteresis is entirely an expression of conventional field-aided (non-thermally-activated) wall displacements. Our understanding of domain structure and magnetization processes in magnetite in the crucial 1–15 μm size interval clearly has a long way to go.

Acknowledgments

Discussions with numerous colleagues, both proponents and opponents of PSD moments, has encouraged us in our pursuit of thermal fluctuation analysis. R. T. Merrill and S. K. Banerjee reviewed the manuscript and offered helpful criticism. The data of Fig. 4, upon whose precision the analysis hinges, were measured by C. Blackburn. Financial support has been provided by the National Research Council of Canada.

References

Adamson, A. W., 1967. *Physical chemistry of surfaces*, Interscience, New York.

Amar, H., 1958. Magnetization mechanism and domain structure of multi-domain particles, *Phys. Rev.*, 111, 149–153.

Bailey, M. E., 1975. The magnetic properties of pseudo single domain grains, *MSc thesis, University of Toronto.*

Bean, C. P., 1955. Hysteresis of mixtures of ferromagnetic micropowders, *J. appl. Phys.*, 26, 1381–1383.

Bean, C. P. & Livingston, J. D., 1959. Superparamagnetism, *J. Appl. Phys.*, 30, 120S–129S.

Bina, M-M., 1966. Contribution à l'étude de l'aimantation thermorémanante portée par des roches, des terres cuites et des minéraux magnétiques naturels ou synthétiques, *Thèse de doctorat, Université de Paris.*

Bina, M-M., 1971. Effet de l'agitation thermique sur la résistance de l'aimantation thermorémanente au traitement par champs alternatifs, *Ann. Geophys.*, 27, 447–451.

Bina, M-M., Manenc, J. & Voeltzel, J., 1966. Sur la thermorémanence d'échantillons de magnétite pure préparée par décomposition de protoxyde de fer, *C.R. Acad. Sci., Paris*, 262, 244–247.

Butler, R. F. & Banerjee, S. K., 1975. Theoretical single-domain grain size range in magnetite and titanomagnetite, *J. geophys. Res.*, 80, 4049–4058.

Craik, D. J. & Isaac, E. D., 1960. Magnetic interaction domains, *Proc. Phys. Soc.*, 76, 160–162.

Day, R., 1973. The effect of grain size on the magnetic properties of the magnetite-ulvospinel solid solution series, *PhD thesis, University of Pittsburgh.*

Dunlop, D. J., 1965. Grain distributions in rocks containing single domain grains, *J. Geomag. Geoelec., Kyoto*, 17, 459–471.

Dunlop, D. J., 1973a. Theory of the magnetic viscosity of lunar and terrestrial rocks, *Rev. Geophys. Space Phys.*, 11, 855–901.

Dunlop, D. J., 1973b. Thermoremanent magnetization in submicroscopic magnetite, *J. geophys. Res.*, 78, 7602–7613.

Dunlop, D. J., 1973c. Superparamagnetic and single-domain threshold sizes in magnetite, *J. geophys. Res.*, 78, 1780–1793.

Dunlop, D. J., 1976. Thermal fluctuation analysis, a new technique in rock magnetism, *J. geophys. Res.*, 81, 3511–3617.

Dunlop, D. J., 1977. Magnetic hysteresis of single-domain and two-domain iron oxides, *in preparation.*

Dunlop, D. J., Stacey, F. D. & Gillingham, D. E. W., 1974. The origin of thermoremanent magnetization: contribution of pseudo-single-domain magnetic moments, *Earth planet Sci. Lett.*, 21, 288–294.

Dunlop, D. J. & Waddington, E. D., 1975. The field dependence of thermoremanent magnetization in igneous rocks, *Earth planet. Sci. Lett.*, 25, 11–25.

Dunlop, D. J. & West, G. F., 1969. An experimental evaluation of single domain theories, *Rev. Geophys. Space Physics*, 7, 709–757.

Fletcher, E. J. & Banerjee, S. K., 1969. High temperature dependence of single crystal anisotropy constants of titanomagnetites (abstract), *EOS, Trans. Am. geophys. Un.*, 50, 132.

Frei, E. H., Shtrikman, S. & Treves, D., 1957. Critical size and nucleation field of ideal ferromagnetic particles, *Phys. Rev.*, 106, 446–455.

Gillingham, D. E. W. and Stacey, F. D., 1971. Anhysteretic remanent magnetization (A.R.M.) in magnetite grains, *Pure appl. Geophys.*, 8, 160–165.

Gustard, B. & Köster, E., 1967. Magnetic phenomena research, *Franklin Institute Technical Reports*, US Army Electronics Command contract DAAB-03-67-C-0095, interim report I-C1932-1.

Gustard, B. & Köster, E., 1968. Magnetic phenomena research, *Franklin Institute Technical Reports*, US Army Electronics Command contract DAAB-03-67-C-0095, final report F-C1932.

Klapel, G. D. & Shive, P. N., 1974. High-temperature magnetostriction of magnetite, *J. geophys. Res.*, 79, 2629–2633.

Kneller, E. F. & Luborsky, F. E., 1963. Particle size dependence of coercivity and remanence of single-domain particles, *J. appl. Phys.*, 34, 656–658.

Kneller, E. & Wohlfarth, E. P., 1966. Effect of thermal fluctuations on the anhysteretic process in ferromagnetic fine-particle assemblies, *J. appl. Phys.*, 37, 4816–4818.

Larson, E. E., Ozima, M., Ozima, M., Nagata, T. & Strangway, D. W., 1969. Stability of remanent magnetization of igneous rocks, *Geophys. J. R. astr. Soc.*, 17, 263–292.

Levi, S., 1974. Some magnetic properties of magnetite as a function of grain size and their implications for paleomagnetism, *PhD thesis, University of Washington*, Seattle.

Luborsky, F. E., 1961. Development of elongated particle magnets, *J. appl. Phys.*, 32, 171S–183S.

McNab, T. K., Fox, R. A. & Boyle, A. J. F., 1968. Some magnetic properties of magnetite (Fe_3O_4) microcrystals, *J. appl. Phys.*, 39, 5703–5711.

Nagata, T., 1961. *Rock magnetism*, Maruzen, Tokyo.

Néel, L., 1949. Théorie du traînage magnétique des ferromagnétiques en grains fins avec applications aux terres cuites, *Ann. Géophys.*, 5, 99–136.

Néel, L., 1950. Théorie du traînage magnétique des substances massives dans le domaine de Rayleigh, *J. Phys. Radium*, 11, 49–61.

Néel, L., 1955. Some theoretical aspects of rock magnetism, *Adv. Phys.*, 4, 191–242.

Néel, L., 1956. Remarques sur la théorie des propriétés magnétiques des couches minces et des grains fins, *J. Phys. Radium*, 17, 250–255.

Parry, L. G., 1965. Magnetic properties of dispersed magnetite powders, *Phil. Mag.*, 11, 303–312.

Pauthenet, R. & Bochirol, L., 1951. Aimantation spontanée des ferrites, *J. Phys. Radium*, 12, 249–251.

Roquet, J., 1954. Sur les rémanences des oxydes de fer et leur intérêt en géomagnétisme, *Ann. Géophys.*, 10, 226–247 and 282–325.

Schmidt, V. A., 1976. The variation of the blocking temperature in models of thermoremanence, *Earth planet. Sci. Lett.*, 29, 146–154.

Shive, P. N., 1969. The effect of internal stress on the thermoremanence of nickel, *J. geophys. Res.*, 74, 3781–3788.

Soffel, H., 1971. Single domain–multidomain transition in natural intermediate titanomagnetites, *Z. Geophys.*, 37, 451–470.

Stacey, F. D., 1963. The physical theory of rock magnetism, *Adv. Phys.*, 12, 45–133.

Stacey, F. D. & Banerjee, S. K., 1974. *The physical principles of rock magnetism*, Elsevier, New York.

Stacey, F. D. & Wise, K. N., 1967. Crystal dislocations and coercivity in fine grained magnetite, *Aust. J. Phys.*, 20, 507–513.

Street, R. & Woolley, J. C., 1949. A study of magnetic viscosity, *Proc. Phys. Soc.*, A62, 562–572.

Syono, Y., 1965. Magnetocrystalline anisotropy and magnetostriction of Fe_3O_4–Fe_2TiO_4 series with special application to rock magnetism, *Jap. J. Geophys.*, 4, 71–143.

Vicena, F., 1955. On the influence of dislocations on the coercive force of ferromagnetics, *Czech. J. Phys.*, 5, 480–501.

West, G. F. & Dunlop, D. J., 1971. An improved ballistic magnetometer for rock magnetic experiments, *J. Sci. Instr.*, 4, 37–40.

Wohlfarth, E. P., 1961. Thermal fluctuation effects in thin magnetic films, *J. Electronics Control*, 10, 33–37.

Appendix: The Néel relaxation equation – an exact analysis

Néel (1949) gives expressions for the relaxation times $\tau(0, \pi)$, $\tau(\pi, 0)$ for thermally activated rotations respectively away from and towards the direction favoured by a positive applied field:

$$\frac{1/\tau(0, \pi)}{1/\tau(\pi, 0)} = f_0 \exp\left[\frac{-\tfrac{1}{2}\upsilon J_s H_K}{kT}\left(1 \pm \frac{H}{H_K}\right)^2\right] \tag{A1}$$

the symbols being the same as in equation (2) of the text. The resultant relaxation time for magnetization change is, therefore,

$$\frac{1}{\tau} = \frac{1}{\tau(0, \pi)} + \frac{1}{\tau(\pi, 0)} = \beta(|H|) f_0 \exp\left[\frac{-\tfrac{1}{2}\upsilon J_s H_K}{kT}\left(1 - \frac{|H|}{H_K}\right)^2\right] \tag{A2}$$

which is identical with equation (2) except for the factor $\beta(|H|) = 1 + \exp(-2vJ_s|H|/kT)$.

If $|H| \gg 2.3kT/vJ_s$, $1 < \beta < 1 + \exp(-4.6) = 1.01$, and to within 1 per cent equation (A2) reduces to equation (2). If $H = 0$, $\beta = 2$ and for $0 < |H| < 2.3kT/vJ_s$, $1 < \beta < 2$. In the text, $\beta = 1$ is assumed for *all* H. Let us see what *maximum* error in the calculated activation volume is introduced by this assumption.

Equation (5) should be replaced by

$$\frac{\langle H_C \rangle}{j_s} = \langle H_{K0} \rangle - \left[\frac{2k \ln(\beta f_0 t)}{J_{S0}}\right]^{1/2} \langle H_{K0}^{1/2} \rangle \langle v_{act}^{-1/2} \rangle \frac{T^{1/2}}{j_s} \qquad \text{(A3)}$$

Assuming $f_0 = 10^9\,s^{-1}$ and $t = 100$ s, $\ln(\beta f_0 t)$ changes from 25.3 (as assumed in the text) to 26.0 if $\beta = 2$ instead of 1, an increase of about 3 per cent. For a given determination of slope from a graph of $\langle H_C \rangle / j_s$ versus $T^{1/2}/j_s$ (e.g. Figs 2 and 5), $\langle v_{act} \rangle$ is, therefore, low by 3 per cent at most and $\langle d_{act} \rangle$ is 1 per cent low at most. (As in the text, $\langle v_{act}^{-1/2} \rangle \approx \langle v_{act} \rangle^{-1/2}$ has been assumed.)

The error made in assuming $\beta = 1$ for all H is comparable to that made in ignoring the dependence of f_0 on H and T (Néel 1949). Equations (2) and (5) are sufficiently exact for practical purposes, in view of the inherent noise in the data from which slopes are determined.

There is one further possible complication. For a given H or H_C, equations (2) and (5) may be exact ($\beta = 1$) at low temperatures but inexact ($\beta > 1$) at high temperatures. A graph in the form of equation (5) will then be slightly non-linear. For interest, Table 5 shows values of the field $|H| = 2.3kT/vJ_s$ below which equations (2) and (5) become inexact for magnetite cubes similar in size to those in the present study. Calculations were done both for room temperature and for 500°C where $j_s \approx 0.5$.

Table 5. Calculated minimum fields below which equations (2) and (5) should be replaced by the exact equations (A2) and (A3).

d (A) (cubes)	$\lvert H\rvert = 2.3kT/vJ_s$ (Oe)	
	20°C	500°C
500	1.5	8.5
750	0.5	2.5
1000	0.2	1.0
2000	<0.1	≈0.1

The minimum H_C values plotted in Fig. 2 were 10–20 Oe at $T = 550$°C. The only deviation from equation (5), and that a few per cent at most, would be expected in the finest grains (sample 4) at temperatures above 500°C.

We are grateful to Dr R. T. Merrill for pointing out the need for a discussion of the approximations made in arriving at equations (2) and (5) and their effect on the thermal fluctuation analysis technique.